Original article
DOI: https://doi.org/10.18721/JPM.15313

INFLUENCE OF THE HYDROGEN SKIN EFFECT ON THE NATURE OF THE FRACTURE OF STEEL SPECIMENS

Yu. S. Sedova✉, *N. M. Bessonov, V. A. Polyanskiy*

Institute for Problems in Mechanical Engineering of the Russian Academy of Sciences,

St. Petersburg, Russia

✉ sedova.yus@mail.ru

Abstract. The influence of hydrogen saturation of steel specimens on the results of their standardized testing for resistance to hydrogen cracking has been carried out. The simulation took into account the hydrogen skin effect observed when metal samples being charged with hydrogen in various electrolyte solutions. The classical decohesion model of hydrogen embrittlement HEDE was used. It was shown that, despite the microscopic skin depth, the effect led to a dual fracture pattern, when the specimen's cross-sectional view exhibited both a hydrogen brittleness area and a normal destruction one. The comparison of calculated results with experimental ones showed the strong influence of the hydrogen skin layer on the results of standardized metal testing. This skin effect plays a significant role in the destruction propagation over a metal sample and should be taken into account when conducting industrial tests, simulations and experimental studies.

Keywords: hydrogen-induced cracking, decohesion, hydrogen charged sample, hydrogen diffusion, destruction

Funding: The reported study was funded by Russian Science Foundation (Project No. 18-19-00160)

Citation: Sedova Yu. S., Bessonov N. M., Polyanskiy V. A., Influence of the hydrogen skin effect on the nature of the fracture of steel specimens, St. Petersburg State Polytechnical University Journal. Physics and Mathematics, Vol. 15, No. 3. 169–184. DOI: https://doi.org/10.18721/JPM.15313

Научная статья
УДК 539.561
DOI: https://doi.org/10.18721/JPM.15313

ВЛИЯНИЕ ВОДОРОДНОГО СКИН-ЭФФЕКТА НА ХАРАКТЕР РАЗРУШЕНИЯ СТАЛЬНЫХ ОБРАЗЦОВ

Ю. С. Седова✉, *Н. М. Бессонов*, *В. А. Полянский*

Институт проблем машиноведения Российской академии наук,

Санкт-Петербург, Россия

✉ sedova.yus@mail.ru

Аннотация. Исследовано влияние насыщения водородом стальных образцов на результаты их стандартизованного тестирования на стойкость к водородному растрескиванию. При моделировании учтен водородный скин-эффект, который наблюдается при стандартизованном насыщении образцов водородом в различных растворах электролитов. Использована классическая декогезионная модель водородной хрупкости HEDE. Показано, что, несмотря на микроскопическую глубину скин-слоя, скин-эффект приводит к двойственному характеру разрушения, когда на изломе образца наблюдаются как площадки водородной хрупкости, так и области обычного разрушения. Сопоставление расчетных результатов с экспериментальными показало сильное влияние водородного скин-слоя на результаты стандартизованного тестирования металлов. Этот скин-эффект играет существенную роль в распространении процесса разрушения по металлическому образцу и должен приниматься во внимание при проведении промышленных испытаний, моделирования и экспериментальных исследований.

Ключевые слова: водородный скин-эффект, индуцированное растрескивание, декогезия, насыщение водородом, диффузия водорода

Финансирование: Исследование выполнено при финансовой поддержке гранта Российского научного фонда (проект №00160-19-18).

Ссылка для цитирования: Седова Ю. С., Бессонов Н. М., Полянский В. А. Влияние водородного скин-эффекта на характер разрушения стальных образцов // Научно-технические ведомости СПбГПУ. Физико-математические науки. 2022. Т. 15. № 3. С. 169–184. DOI: https://doi.org/10.18721/JPM.15313

Introduction

The so-called metallurgical dissolved hydrogen accumulates in metals and metal products during the manufacturing process. It negatively affects all mechanical and technological characteristics of metals, is one of the main causes of embrittlement, porosity and flaking in rolled products. Production facilities introduce different measures for monitoring the concentration of metallurgical hydrogen. It is maintained at a level of about $1{,}000{,}000^{-1}$ or less in steels and aluminum alloys.

The second source of dissolved hydrogen is an aggressive external environment to which metal parts are exposed during operation. Any corrosion process is accompanied by release of hydrogen and its absorption inside the metal. External mechanical loads and the presence of pure hydrogen in the environment can considerably accelerate hydrogen degradation of metal properties.

A system for standardized testing for resistance to hydrogen-induced cracking (HIC) has been developed and implemented in the manufacturing industry over the recent decades [1–3]. Typically, the procedure consists of an exposure phase (hydrogen saturation) of metal specimens

in a corrosive environment that lasts up to 100 h. The second phase consists of mechanical tests and microscopic studies of the specimens: the surfaces of fractures and cracks induced by hydrogen are recorded.

These tests allow to achieve high resistance to HIC in modern pipe steels. While hydrogen-induced cracks tended to evolve inside steel specimens tested by the procedures developed in the 1970s [4], modern steels are characterized by only minor microcracking. At the same time, the mechanical characteristics of the specimens considerably deteriorate after saturation with hydrogen, and high-strength steels are characterized by a proportional decrease in crack resistance [5, 6]. Numerous fractographic studies [7–10], carried out experimentally for steels fractured during mechanical tests, indicate the presence of two characteristic fracture regions: brittle and ductile. Modern alloys are widely used in various fields of energy and manufacturing industries. Therefore, the effect of their rapid degradation upon saturation with hydrogen should be investigated and mitigated.

The mean partial concentration of hydrogen atoms to matrix atoms in the metal increases to no more than 1:30,000 during HIC testing [11]. Furthermore, recent studies have observed a skin effect of hydrogen saturation in aqueous corrosive solutions during cathodic polarization, where all hydrogen absorbed by the metal is concentrated in a thin surface layer of specimens about 50–100 μm thick [12–15]. If the working diameter of the specimen is 8–10 mm, this layer can be attributed to layers with small thickness (the ratio of 1:100 is typical for theory of thin shells). Thus, from a mechanical perspective, we are dealing with a problem on the influence of a small parameter.

To date, several approaches have been proposed to describe hydrogen-induced degradation.

One of the first models was Hydrogen-Enhanced Decohesion (HEDE) [16]. It describes brittle fracture resulting from accumulation of hydrogen at the crack tip and development of hydrogen embrittlement without plastic deformations. At the microscopic level, the approach is based on the idea that interstitial hydrogen expands the metal lattice of crystals, thus contributing to a decrease in the adhesion strength of atoms [17]. From the standpoint of energy, hydrogen atoms lower the energy barrier for fracture, which leads to segregation of grains, or decohesion.

A fundamentally different approach to modeling hydrogen degradation of the mechanical properties of materials is taken within the model of hydrogen-enhanced localized plasticity (HELP) [18, 19]. Hydrogen dissolved in the metal is interpreted within this model as a chemical that reduces the energy required to initiate dislocations. It is assumed that 'softening' of the metal, or localized plasticity, is observed at the tip of the crack, where hydrogen is concentrated under the action of internal stresses.

The dual nature of the fracture observed in HIC testing is commonly interpreted by using a combination of both models: HELP + HEDE. Brittle HEDE mechanism is assumed to work if the local hydrogen concentrations in the tip of the crack are above a certain 'switching threshold', and HELP is assumed to apply for concentrations below the threshold one. One of the problems of this approach is the exponential increase (up to 100 times) in hydrogen concentration during plastic deformation, which directly follows from the equations of the HELP model [20]. Thus, if the models are sequentially 'combined', the localized plastic deformation induced by hydrogen should lead to a manifold increase in its local concentration, triggering a mechanism of brittle decohesion for the fracture.

In addition, the HELP model essentially describes an increase in ductility due to a decrease in the yield strength of the material. However, the bulk of the experimental evidence does not suggest a decrease in the yield point during specimen testing [6]. All of this indicates that existing experimental and theoretical data contradict the hypothesis that the HELP model is initiated, determining the principal fracture surface.

These HELP + HEDE paradoxes allow us to settle on a decohesion model of hydrogen cracking.

Description of the model

The modern concept of the HEDE-model comprises the following key elements:

equations of elastic or viscoelastic solid medium with hardening (in particular, for materials with hardening);

equations of diffusion describing the redistribution and accumulation of hydrogen;

dependences describing hydrogen degradation of cohesive parameters.

Hydrogen transport within a solid has been traditionally understood as a diffusive process, and the equation of Fick's second law [21] was used to describe it:

$$\frac{\partial C}{\partial t} = \nabla \cdot \left[D\left(T, \mathbf{r}\right) \nabla C \right], \tag{1}$$

where C is the hydrogen concentration, t is the time, $\mathbf{r}$ is the coordinate vector, D is the diffusion coefficient, T is the absolute temperature, ∇ is the nabla operator.

However, modern approaches typically introduce components accounting for the thermodynamic or chemical potential [22]:

$$\mu = \mu_0 \left(T\right) + RT \ln C - V_H p.$$

In this case, Eq. (1) takes the form

$$\frac{\partial C}{\partial t} = \nabla \cdot \left[D\left(T, \mathbf{r}\right) \left(\nabla C - \frac{C V_H}{RT} \nabla p \right) \right], \tag{2}$$

and the following form accounting for the effect of mechanical stresses:

$$\frac{\partial C}{\partial t} = D \nabla^2 C - \frac{D V_H}{RT} \nabla C \cdot \nabla p - \frac{D C V_H}{RT} \nabla^2 p, \tag{3}$$

where p is the pressure in spherical stress tensor, V_{H} is the partial molar volume of hydrogen [23].

According to Gorsky's law [24], hydrogen tends to migrate to regions of maximum tensile stresses. An increase in its concentration in these regions unavoidably lowers the cohesion of the crack edges, which is what leads to decohesion [16]. The model characterizes this phenomenon by introducing the parameter θ for the degree to which the free surface of crack edges is filled with hydrogen atoms:

$$\theta = \frac{C}{C + \exp\left(-\frac{\Delta g_H}{RT} \right)}, \tag{4}$$

where Δg_{H} is the difference in Gibbs free energy for hydrogen between the state adsorbed inside the crystal lattice and the free state (established experimentally).

This expression was proposed by Serebrinsky [24] based on the thermodynamic relationship for the partial molar volume of hydrogen inside and on the surface of a single crystal, obtained by McLean [25].

Notably, if the partial volume of impurity is used in this relationship, accounting for the value of C (10^{-6}), expression (4) takes the form:

$$\theta = \frac{55.85 \cdot C \cdot 10^{-6}}{55.85 \cdot C \cdot 10^{-6} + \exp\left(-\frac{\Delta g_H}{RT} \right)}. \tag{5}$$

The value of the parameter θ allows calculating the specific energy $\gamma(\theta)$ of the free surface, depending on the sorption of hydrogen on it. Most existing studies use the formula proposed by Serebrinsky to describe this relationship [25]:

$$\gamma\left(\theta\right) = \left(1 - 1.0467\theta + 0.1687\theta^2\right) \gamma\left(0\right), \tag{6}$$

where $\gamma(0)$ is the surface energy in the absence of hydrogen.

Next, the brittle fracture model takes into account the identity for energy

$$G = 2\gamma(\theta) = f(\sigma_{Zc}, \delta_c), \tag{7}$$

where G is the fracture energy; $f(\sigma_{Zc},\delta_c)$ is a linear function depending on the maximum cohesive stresses σ_{Zc} normal to the crack edges, and on the maximum relative displacements δ_c of the crack edges at which the bonds between them do not break (or decohesion does not occur).

The form of the function $f(\sigma_{Zc},\delta_c)$ is determined by the cohesive law.

Assuming the value of δ_c to weakly depend on the value of θ, the HEDE-model introduces the law of hydrogen degradation:

$$\sigma_{Zc}(\theta) = \left(1 - 1.0467\theta + 0.1687\theta^2\right)\sigma_Z(0), \tag{8}$$

where $\sigma_Z(0)$ are cohesive stresses, normal to the crack edges acting in the absence of hydrogen.

According to the criterion for initiation and propagation of the crack by the HEDE mechanism, the crack preserves its configuration as long as the level of elastic stresses normal to its edges and acting near the tip of the crack does not exceed the cohesive stresses bridging the crack. As soon as the hydrogen accumulated at the tip of the crack under the action of chemical potential reduces these stresses so that this condition is violated, the crack starts to grow, with a new free surface forming. On the other hand, this cracking produces a local increase in the level of normal stresses in the new position of the crack tip, in turn leading to an increase in the local hydrogen concentration. The cohesive stresses once more decrease to a value violating the condition for crack stability, and the process is repeated again and again.

On the other hand, the energy required for fracture can be expressed in terms of material parameters. For a crack opening normally, it can be written as

$$G = \frac{K_{Ic}^2}{\hat{E}}, \tag{9}$$

where K_{Ic} is the critical stress intensity factor acting in the vicinity of the crack tip; the quantity $K = E(1 - \nu^2)$ is either $K = E$ for the cases of plane stress or plane strain state, respectively (E is Young's modulus, ν is Poisson's ratio).

In view of identity (7), we can prove that a decrease in the specific energy of the free surface due to an increase in the hydrogen concentration also leads to a decrease in K_{Ic}:

$$\frac{K_{Ic}^2}{K_{Ic}^2(0)} = \frac{\gamma(\theta)}{\gamma(0)} = 1 - 1.0467\theta + 0.1687\theta^2.$$

Thus, the magnitude of the critical stress intensity factor (the parameter characterizing the crack resistance of the material) depends on the hydrogen concentration as

$$K_{Ic}(\theta) = \sqrt{1 - 1.0467\theta + 0.1687\theta^2}\, K_{Ic}(0), \tag{10}$$

where $K_{Ic}(0)$ is the experimentally established value of crack resistance in the material in the absence of hydrogen.

It follows that the presence of hydrogen dissolved in the material modifies the force criterion of Irvine fracture ($K_I = K_{Ic}$) [27, 28], so cracking becomes possible at a lower value of K_I.

Problem statement

We consider a problem on uniaxial stretching of a cylindrical rod with an elliptical notch, saturated with hydrogen. We refrained from using standard finite element packages with in-built modules for cohesive zone modeling and crack propagation, since specialized fictitious cohesive elements have to be introduced in them following a particular cohesive law. This means that a large number of additional model parameters have to be introduced and several additional assumptions have to be adopted.

The model was implemented with the C++ code developed in Microsoft Visual Studio, allowing to obtain numerical solutions to problems on the stress-strain state of bodies using the finite volume method.

The procedure comprised two consecutive stages.

Stage 1. The problem on the stress-strain state in a pre-stretched specimen is solved.

Stage 2. The diffusion problem on the redistribution of hydrogen along the rod is solved.

As part of the second stage, the cohesive stresses σ_{Zc} and the crack resistance parameter K_{Ic} were also calculated.

A system of equations (11)–(13) from linear elasticity theory was solved at the first stage of the problem. The system includes a differential equilibrium equation (11), equation for the linear strain tensor (12) and generalized Hooke's law (13):

$$\begin{cases} \nabla \cdot \boldsymbol{\sigma} + \mathbf{f} = 0, & (11) \\ \boldsymbol{\varepsilon} = \dfrac{1}{2}\left(\nabla \mathbf{u} + \mathbf{u}\nabla\right), & (12) \\ \boldsymbol{\sigma} = \lambda\theta\mathbf{E} + 2G\boldsymbol{\varepsilon}, & (13) \end{cases}$$

where $\boldsymbol{\sigma}$ is the Cauchy stress tensor; $\mathbf{f}$ is the body force intensity; $\mathbf{u}$ is the displacement vector; λ, G are the Lamé parameters; $\theta = \mathrm{tr}(\varepsilon)$ is the relative volume change for the hydrostatic pressure $p = 1/3\mathrm{tr}(\sigma)$.

A method proposed by Wilkins [28] was used to numerically solve Eq. (11).

The characteristics of the stress-strain state of the specimen obtained in the first step of the technique were recorded in the second stage. Eqs. (3), (5), (8) and (10) that we described earlier were solved.

$$\begin{cases} \dfrac{\partial C}{\partial t} = D\nabla^2 C - \dfrac{DV_H}{RT}\nabla C \cdot \nabla p - \dfrac{DCV_H}{RT}\nabla^2 p \\ \theta = \dfrac{55.85 \cdot C \cdot 10^{-6}}{55.85 \cdot C \cdot 10^{-6} + \exp\left(-\dfrac{\Delta g_H}{RT}\right)} \\ \sigma_{Zc}(\theta) = \left(1 - 1.0467\theta + 0.1687\theta^2\right)\sigma_Z(0) \\ K_{Ic}(\theta) = \sqrt{1 - 1.0467\theta + 0.1687\theta^2}\, K_{Ic}(0). \end{cases}$$

Eq. (3) was also numerically solved based on Wilkins's determination method [29].

The instantaneous SIF in the vicinity of the crack tip was calculated from the approximate Benthem–Koiter formula [30, 31], obtained for the case of a crack with the length c initiating in an edge notch in a cylindrical rod with the diameter D under the action of uniaxial tension σ^{∞}_{z}:

$$\sigma_{net} = \sigma_Z^{\infty}\left(\frac{D}{d}\right)^2. \quad (14)$$

The conditions for cracking were found based on the results obtained in the second stage by the criterion for cohesive stresses or the Irwin force criterion for fracture.

We selected the model relying on the experimental data to be able to compare and evaluate the results obtained by the finite-volume solution. We were guided by a recently published study [8], investigating the effect of hydrogen on the properties of chromoly steel. The article considers a specimen of 2.25Cr1Mo ferritic steel shaped as a cylindrical rod 9.0 mm in diameter with a radial notch 2.0 mm deep, 1.2 mm wide and with a rounding radius of 0.15 mm.

Fractographic images of the fracture surface obtained after tensile tests of the specimen pre-saturated with hydrogen by cathodic polarization revealed a circular region of brittle fracture w up to 1 mm wide and an internal region of ductile fracture.

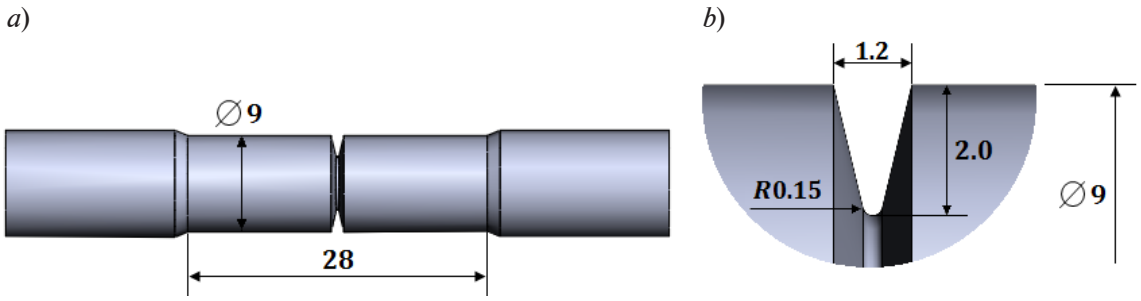

Fig. 1. Image of cylindrical steel specimen with radial notch (*a*)
and its half cross-section at the notch root (*b*) (dimensions are given in mm)

We considered uniaxial tension of a cylindrical rod of the same geometry (Fig. 1), made of the same steel (the tensile load was 650 MPa). The computations were carried out in a two-dimensional axisymmetric formulation. By virtue of symmetry, the geometry of the modeled specimen was a quarter of the longitudinal section of the bar (Fig. 2).

The following properties of the 2.25Cr1Mo steel were used in the computations:

Physical properties of 2.25Cr1Mo steel

Yield strength σ_B	895 MPa
Flow stress σ_T	761 MPa
Density ρ	7,750 kg/m^3
Shear modulus μ	80 GPa
Poisson's ratio ν	0.3
Bulk modulus of elasticity K	140 GPa
Fracture toughness $K_{Ic}(0)$	64.1 MPa·m$^{1/2}$

Let us also give the values of the remaining computational parameters. The diffusivity was assumed to be constant, amounting to $D = 2 \cdot 10^{-11}$ m^2/s; the partial molar volume of hydrogen $V_H = 2 \cdot 10^{-6}$ m^3/mol [32]; the difference in Gibbs free energies for the state of hydrogen adsorbed inside the crystal lattice and its free state was $\Delta g_H = 30$ kJ/mol [32], the absolute temperature $T = 298$ K. The magnitude of the stresses included in Eq. (8), taking into account the recommendations from [33], was assumed to be $\sigma_z(0) = 30\ \sigma T$.

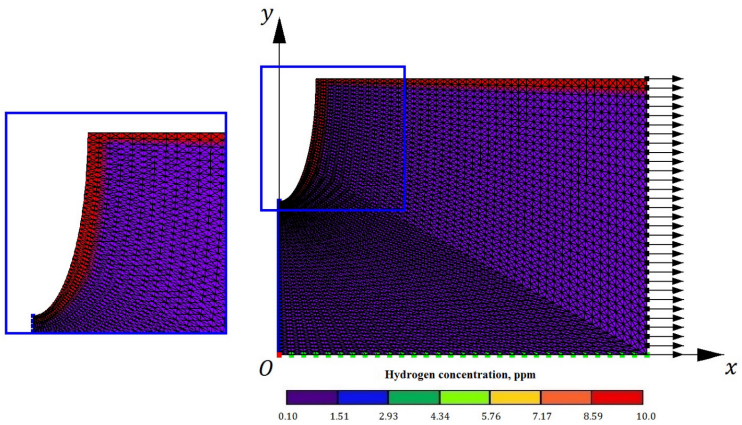

Fig. 2. Computational finite-volume model for a quarter of longitudinal section
of the bar (see Fig. 1,*a*); geometry, boundary and initial conditions are shown
the arrows indicate the direction of extension

The initial distribution of hydrogen over the specimen was established as follows: uniform background concentration $\tilde{c}_0 = 0.1 \cdot 10^{-6}$ throughout the region and the concentration $c_0 = 10 \cdot 10^{-6}$ in the surface layer with a thickness of one structural element ($t = 20$ μm). The latter characterizes the experimentally observed hydrogen concentration in metal specimens, accumulating on the surface. (hydrogen saturation due to the skin effect), see enlarged fragment in Fig. 2.

By virtue of symmetry, displacement along the horizontal axis *Ox* is prohibited for the left face, and displacement along the vertical axis *Oy* for the bottom face. A tensile stress σ acting along the axis *Ox* was applied to the right edge of the region.

The initiation and propagation of the crack was modeled as follows. After the characteristics of the body's stress-strain state are obtained, analysis of the diffusion problem on the redistribution of hydrogen over the specimen was performed at the second stage of the computational technique. The behavior of two inequalities was monitored in the analysis: $\sigma_{el} < \sigma_{Zc}(\theta)$ for stresses and $K_I < K_{Ic}(\theta)$ for SIFs at the nodes of the finite-volume mesh along the hypothetical line of crack propagation line (along the left face of the region). As soon as one of these inequalities was violated in the node due to an increase in hydrogen concentration or an increase in the level of elastic stresses, the restriction on displacements along the horizontal axis *Ox* was removed in this node, reproducing a broken bond with the node at the opposite edge of the crack. The node could then move freely under the applied load.

Results of finite-element modeling

Fig. 3 shows the dependence for the time range between the instants when the fracture criterion is satisfied in two consecutive nodes of the finite volume model. This is a time range necessary for hydrogen to redistribute under the influence of elastic stresses and subsequently accumulate in the given node, with the resulting decrease in cohesive stresses σ(θ) or the crack resistance parameter of the material $K_{Ic}(\theta)$.

It is evident from Fig. 3 that the criterion for bond breakage by the decohesion mechanism is instantly fulfilled in the first two nodes of the mesh. This is due to high content of hydrogen in the surface layer of the specimen, so the cohesive stresses bridging the nodes of the material are greatly reduced as a result, and fracture by the HEDE mechanism occurs at the first time step of the problem solution. The distributions of the components of elastic stresses acting along the horizontal axis and the hydrogen content in the vicinity of the crack tip at different times are shown in Figs. 4 and 5, respectively.

However, the time for diffusion increases with distance from the specimen surface, with the process reflected accordingly in the solution of the diffusion problem. A certain amount of time has to pass for hydrogen to be redistributed, diffused and accumulated in the current crack tip until the facture criterion is satisfied. For this reason, the dependence is shown by an increasing segment starting from the third node (see Figs. 4,*b* and 5,*b*), but the propagation of the crack still follows a HEDE fracture mechanism.

This scenario continues until the sixth node of the mesh. After that, elastic stresses (see Fig. 4,*c*) acting near the stress concentrator start to exert a considerable effect. Their values gradually increase, so it is sufficient to decrease the cohesive stresses initiated by hydrogen to a smaller degree to trigger the decohesion mechanism (see Fig. 5,*c*). Consequently, an ever shorter time is required to solve the diffusion problem.

Notably, the value of the crack resistance parameter also decreases substantially at this stage of monitoring due to the presence of hydrogen in the material, but it still turns out to be higher than the value of the SIF acting near the crack tip.

As seen from Fig. 3, the decreasing trend in the critical hydrogen concentration at which decohesion occurs continues with distance from the specimen surface. At the same time, the magnitude of elastic stresses acting at the tip of the crack becomes so large at a distance of about 0.97 mm (corresponding to the seventeenth node of the mesh) that the crack can propagate further even at a background value of hydrogen content.

After that, the crack extends to a considerable size, so that the SIF reaches a high value near its tip, immediately exceeding the crack resistance of the material (also reduced by the presence of hydrogen in the bar) in the next node, with fracture propagating by only 1.0 mm (see Fig. 4,*d* and 5,*d*). Evidently, as the crack grows further, the level of the active stresses only increases. This explains the observed continuous propagation of the main crack after switching of the fracture mechanism, which happens after the force criterion for fracture is satisfied.

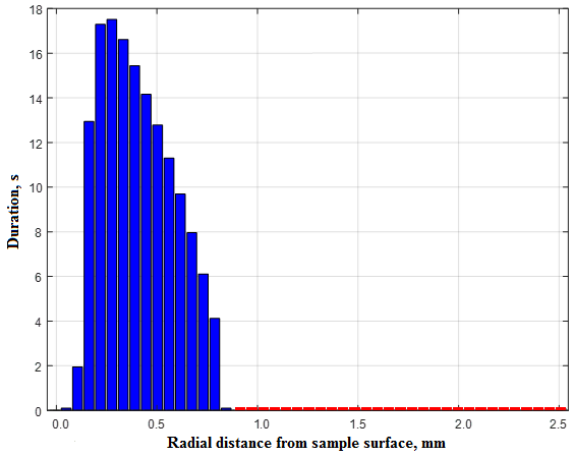

Fig. 3. Time required for the crack to propagate over 1 mesh spacing as a function of distance from the specimen surface
decohesion mechanism and crack resistance are shown in blue and red, respectively

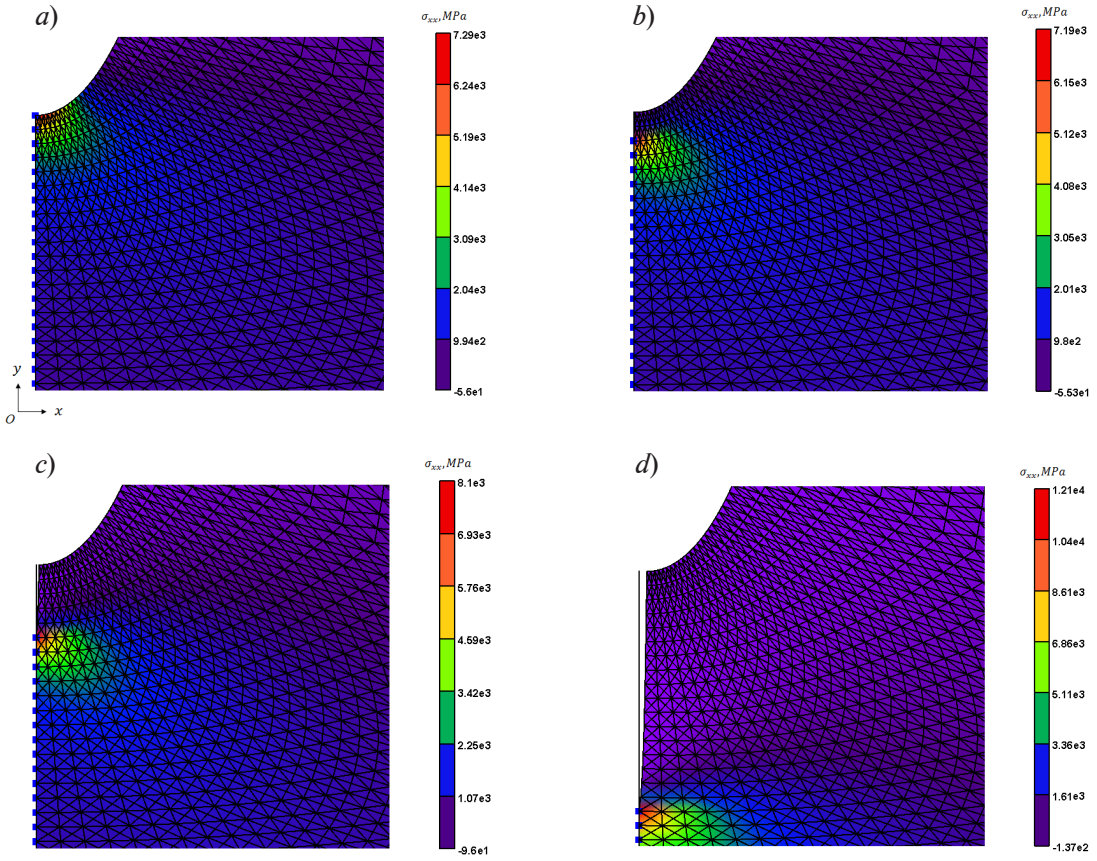

Fig. 4. Distributions of elastic stress components (MPa) acting in the horizontal direction at different time instants when decohesion is observed in the first (*a*), third (*b*), sixth (*c*) mesh nodes; switching of fracture mechanism (*d*)

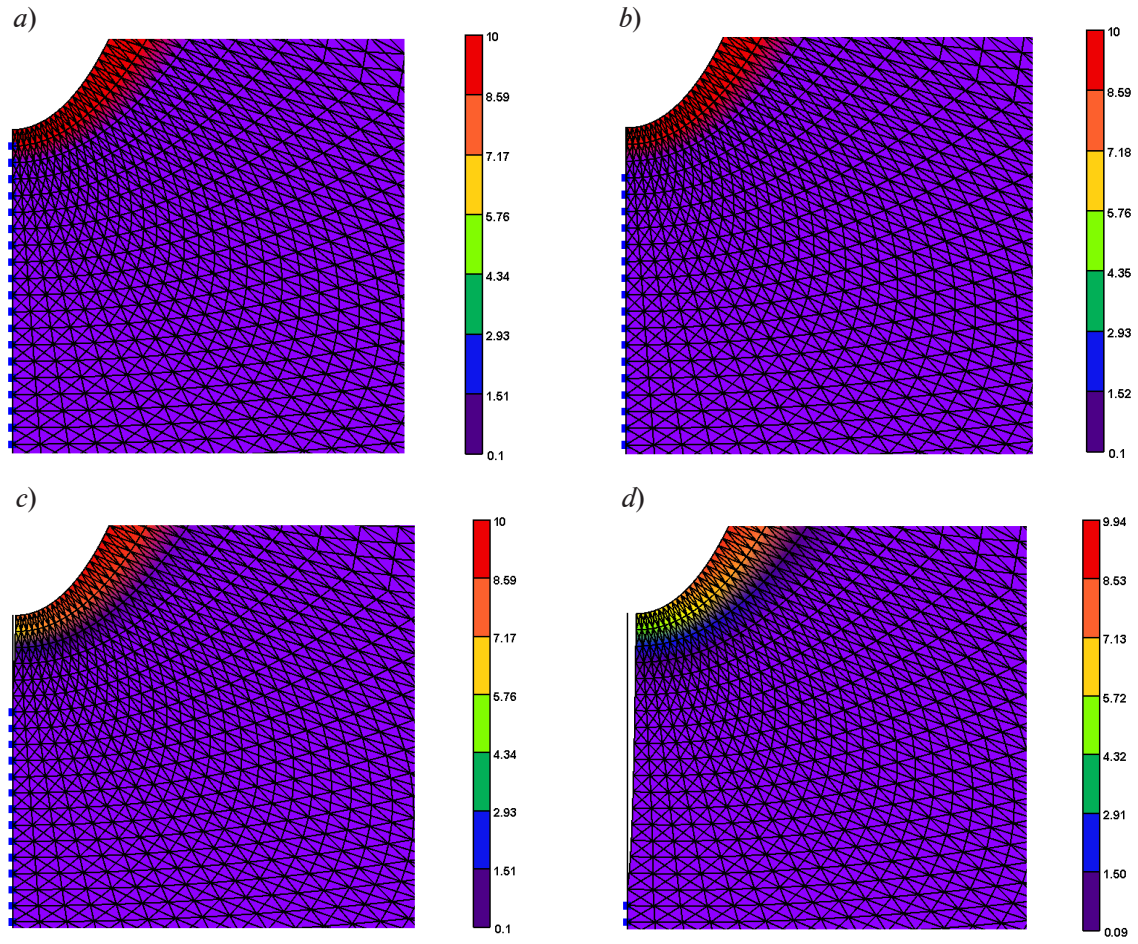

Fig. 5. Distribution of hydrogen concentration (10^{-6}) at the same instants as in Fig. 4

Fig. 6 shows the distribution of hydrogen concentration over the sample radius at crucial moments characterizing the evolution of the process from the initial state to propagation of the crack to half the specimen thickness. Apparently, as the crack propagates, hydrogen gradually redistributes from the surface of the specimen and moves deep into the material under the action of the chemical potential of the applied stresses. Importantly however, the penetration depth does not exceed 1 mm, because further fracture of steel occurs at the initial background hydrogen content, due to high stresses near the crack tip.

Thus, simulating the process allowed detecting and tracking the mechanism relating the saturation of specimens with hydrogen and the nature of fracture in the metal alloy under load (skin effect).

Results and discussion

Let us consider the finite-volume solution of the equations from the classical HEDE model for brittle fracture accounting for the skin effect of hydrogen saturation of the specimens. We adopt the approach of linear cracking theory and a classical model of hydrogen embrittlement. The computational results indicate that fracture follows the brittle decohesion mechanism at first, due to the high concentration of hydrogen in the surface layer. Hydrogen diffuses under the action of both the concentration gradient and the chemical potential along the crack propagation line, but its concentration in the moving crack tip drops to background values due to the slow progress of the diffusion process. At the same time, the balance between the length of the crack induced by hydrogen and the load level is important, since the crack can grow further after reaching a certain critical length with the background concentration of hydrogenby the standard cracking mechanism.

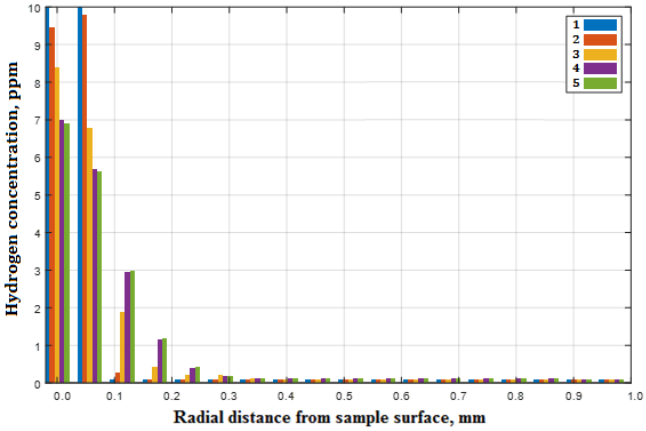

Fig. 6. Distribution of hydrogen concentration over the specimen radius (from the surface to the central axis) at crucial moments in the process: initial state (*1*), decohesion in the 3rd (*2*) and 6th (*3*) mesh nodes, switching of fracture mechanism (*4*) and crack extending to half the specimen thickness (*5*)

The images showing the regions with the distribution of hydrogen over the rod cross-section (Fig. 7) present a clear illustration for the evolution of the given process. Brittle fracture associated with increased hydrogen concentration is observed along the crack edges; sites of hydrogen embrittlement are detected in this region. Normal fracture occurs in the central part of the specimen, in accordance with the cracking theory.

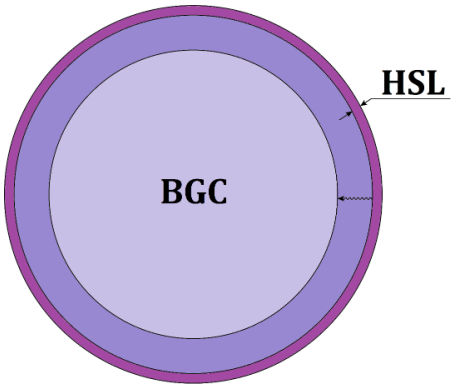

Fig. 7. Schematic representation of hydrogen redistribution regions within the specimen: HSL is the hydrogen skin layer; BHC is the normal (background) hydrogen concentration. The arrow indicates the direction of hydrogen diffusion during crack growth

The simulation results quantitatively and qualitatively agree with the experimental data presented in [8, 34]. The region of hydrogen-induced brittle fracture was 1 mm wide. We carried out computations varying the skin layer thickness, hydrogen concentration and the magnitude of the applied load. The results indicate that this thickness depends only on the level of load applied to the specimen (or the extension rate of the specimen): the larger it is, the smaller the hydrogen embrittlement region. This is qualitatively consistent with the experimental data [35].

Thus, the classical models we used allow describing the critical influence of the skin effect region (a small parameter) with a small volume on the fracture of specimens, relating the experimentally observed dual nature of the fracture in the specimens with the procedure used to saturate them with hydrogen. Our findings can serve to explain the differences between the results for testing steel specimens and for operation of parts and assemblies manufactured from the same steels in aggressive environments.

Conclusion

We have carried out finite-volume simulation for fracture in a cylindrical dumbbell-shaped steel specimen with an elliptical cutout saturated with hydrogen. The mechanism of hydrogen-enhanced decohesion (HEDE) was used as a model of hydrogen embrittlement. The skin effect from saturating the specimens with hydrogen, established experimentally, was taken into account.

The computational results indicate that fracture begins at the surface of the specimen as brittle, initiated by hydrogen. A crack then appears, and, as it reaches a certain length, continues to propagate naturally with typical background values of hydrogen concentration. This change in the nature of fracture produces a dual picture: regions of both hydrogen embrittlement and standard fracture are observed in the specimen cross-section.

Moreover, the simulations revealed that the skin effect in the distribution of hydrogen concentration may be the main reason behind the dual behavior of fracture; on the other hand, the general consensus is that this duality can be attributed to the simultaneously evolving HELP and HEDE mechanisms at the tip of the main crack.

The skin effect from hydrogen charging has a major influence on fracture of metal specimens despite its small depth, so it should definitely be taken into consideration in industrial tests, experimental studies, theoretical analysis, and simulation.

REFERENCES

1. ISO11114-4. Transportable gas cylinders – compatibility of cylinder and valve materials with gas contents – part 4: Test methods for selecting metallic materials resistant to hydrogen embrittlement. ISO 11114-4:2017 International Organization for Standardization, (2017). URL: https://www.iso.org/standard/64587.html (Date of the last access: 12.03.2022).

2. ISO16573. Steel-measurement method for the evaluation of hydrogen embrittlement resistance of high strength steels. ISO 16573:2015 International Organization for Standardization, (2015). URL: https://www.iso.org/standard/57128.html (Date of the last access: 12.03.2022).

3. ISO17081. Method of measurement of hydrogen permeation and determination of hydrogen uptake and transport in metals by an electrochemical technique. ISO 17081:2014 International Organization for Standardization (2014). URL: https://www.iso.org/standard/64514.html (Date of the last access: 12.03.2022).

4. **Giuliani L., Mirabile M., Sarracino M.,** Embrittlement kinetics of N 80 steel in H_2S environment, Metall. Mater. Trans. B. 5 (9) (1974) 2069–2073.

5. **Nagumo M., Yoshida H., Shimomura Y., Kadokura T.,** Ductile crack growth resistance in hydrogen-charged steels, Mater. Trans. 42 (1) (2001) 132–137.

6. **Koyama M., Tasan C. C., Tsuzaki K.,** Overview of metastability and compositional complexity effects for hydrogen-resistant iron alloys: Inverse austenite stability effects, Eng. Fract. Mech. 214 (2019) 123–133.

7. **Troiano A. R.,** The role of hydrogen and other interstitials in the mechanical behavior of metals, Metallogr. Microstruct. Anal. 5 (6) (2016) 557–569.

8. **Peral L. B., Zafra A., Fernández-Pariente I., et al.,** Effect of internal hydrogen on the tensile properties of different CrMo(V) steel grades: Influence of vanadium addition on hydrogen trapping and diffusion, Int. J. Hydrog. Energy. 45 (41) (2020) 22054–22079.

9. **Venezuela J., Hill T., Zhou Q., et al.,** Hydrogen-induced fast fracture in notched 1500 and 1700 MPa class automotive martensitic advanced high-strength steel, Corr. Sci. 188 (1 August) (2021) 109550.

10. **Duportal M., Oudriss A., Savall C., et al.,** On the implication of mobile hydrogen content on the surface reactivity of an austenitic stainless steel, Electrochim. Acta. 403 (20 January) (2022) 139684.

11. **Alekseeva E.**, **Belyaev A.**, **Zegzhda A., et al.,** Boundary layer influence on the distribution of hydrogen concentrations during hydrogen-induced cracking test of steels, Diagnostics, Resource and Mechanics of Materials and Structures. (3) (2018) 43–57 (in Russian).

12. **Polyanskiy V. A., Belyaev A. K., Alekseeva E. L., et al.,** Phenomenon of skin effect in metals due to hydrogen absorption, Contin. Mech. Thermodyn. 31 (6) (2019) 1961–1975.

13. **Martinsson A., Sandström R.,** Hydrogen depth profile in phosphorus-doped, oxygen-free copper after cathodic charging, J. Mater. Sci. 47 (19) (2012) 6768–6776.

14. **Wu R., Ahiström J., Magnusson H., et al.,** Charging, degassing and distribution of hydrogen in cast iron (report SKB R-13-45), Svensk Kärnbränslehantering AB, Swedish Nuclear and Waste Management Co., Stockholm, May 2015.

15. **Oriani R. A.,** A mechanistic theory of hydrogen embrittlement of steels, Berichte der Bundesgesellschaft für physikalische Chemie. 76 (8) (1972) 848–857.

16. **Troiano A. R.,** The role of hydrogen and other interstitials in the mechanical behavior of metals, Trans. ASM. 52 (1960) 54–80.

17. **Birnbaum H. K., Sofronis P.,** Hydrogen-enhanced localized plasticity – a mechanism for hydrogen-related fracture, Mater. Sci. Eng. A. 176 (1–2) (1994) 191–202.

18. **Sofronis P.**, **Birnbaum H. K.,** Mechanics of the hydrogen dislocation-impurity interactions. I. Increasing shear modulus, J. Mech. Phys. Solid. 43 (1) (1995) 49–90.

19. **Taha A., Sofronis P.,** A micromechanics approach to the study of hydrogen transport and embrittlement, Eng. Fract. Mech. 68 (6) (2001) 803–837.

20. **von Fick A.,** Ueber Diffusion, Annalen der Physik. 170 (1) (1855) 59–86.

21. **Shewmon P. G.,** Diffusion in solids, Mc Graw-Hill Book Co, Inc., New York, 1963.

22. **Kolachev B. A.,** Vodorodnaya khrupkost metallov [Hydrogen embrittlement of metals], Metallurgiya, Moscow, 1985 (in Russian).

23. **Gorsky W.,** Theorie der elastischen Nachwirkung in ungeordneten Mischkristallen (elastische Nachwirkung zweiter Art), Physikalische Zeitschrift der Sowjetunion. 8 (1935) 457–471.

24. **Serebrinsky S., Carter E. A., Ortiz M.,** A quantum-mechanically informed continuum model of hydrogen embrittlement, J. Mech. Phys. Solids. 52 (10) (2004) 2403–2430.

25. **McLean D.,** Grain boundaries in metals. Clarendon Press, London, 1957.

26. **Irwin G. R.,** Analysis of stresses and strains near the end of a crack traversing a plate, J. Appl. Mech. 24 (3) (1957) 361–364.

27. **Irwin G. R.,** Fracture, In book: Encyclopedia of Physics, Ed. by S. Flugge, Vol. 6: Elasticity and Plasticity, Springer Verlag, Berlin (1958) 551–590.

28. **Wilkins M. L.,** Computer simulation of dynamic phenomena, Springer Science & Business Media, Berlin, Heidelberg, 1999.

29. Stress intensity factors handbook, in 2 Vols. Editor-in-Chief Murakami Y. Vol. 2. The Society of Materials Science, Pergamon Press Oxford, New York, 1987.

30. **Benthem J. P., Koiter W. T.,** Asymptotic approximations to crack problems, In book: Methods of analysis and solutions of crack problems, Ed. by G. C. Sih, Book Series “Mechanics of Fracture”, Vol. 1. Springer, Dordrecht (1973) 131–178.

31. **Hirth J. P.,** Effects of hydrogen on the properties of iron and steel, Metallurg. Trans. A. 11 (6) (1980) 861–890.

32. **Tvergaard V., Hutchinson J. W.,** The relation between crack growth resistance and fracture process parameters in elastic-plastic solids, J. Mech. Phys. 40 (6) (1992) 1377–1397.

33. **Herms E., Olive J. M., Puiggali M.,** Hydrogen embrittlement of 316L type stainless steel, Mater. Sci. Eng. A. 272 (2) (1999) 279–283.

34. **Momotani Y., Shibata A., Terada D., Tsuji N.,** Effect of strain rate on hydrogen embrittlement in low-carbon martensitic steel, Int. J. Hydrog. Energy. 42 (5) (2017) 3371–3379.

СПИСОК ЛИТЕРАТУРЫ

1. ISO11114-4. Transportable gas cylinders – compatibility of cylinder and valve materials with gas contents – part 4: Test methods for selecting metallic materials resistant to hydrogen embrittlement. ISO 11114-4:2017 International Organization for Standardization, 2017. URL: https://www.iso.org/standard/64587.html (Дата последнего обращения: 12.03.2022).

2. ISO16573. Steel – measurement method for the evaluation of hydrogen embrittlement resistance of high strength steels. ISO 16573:2015 International Organization for Standardization, 2015. URL: https://www.iso.org/standard/57128.html (Дата последнего обращения: 12.03.2022).

3. ISO17081. Method of measurement of hydrogen permeation and determination of hydrogen uptake and transport in metals by an electrochemical technique. ISO 17081:2014 International Organization for Standardization, 2014. URL: https://www.iso.org/standard/64514.html (Дата последнего обращения: 12.03.2022).

4. **Giuliani L., Mirabile M., Sarracino M.** Embrittlement kinetics of N 80 steel in H_2S environment // Metallurgical and Materials Transactions B. 1974. Vol. 5. No. 9. Pp. 2069–2073.

5. **Nagumo M., Yoshida H., Shimomura Y., Kadokura T.** Ductile crack growth resistance in hydrogen-charged steels // Materials Transactions. 2001. Vol. 42. No. 1. Pp. 132–137.

6. **Koyama M., Tasan C. C., Tsuzaki K.** Overview of metastability and compositional complexity effects for hydrogen-resistant iron alloys: Inverse austenite stability effects // Engineering Fracture Mechanics. 2019. Vol. 214. 1 June. Pp. 123–133.

7. **Troiano A. R.** The role of hydrogen and other interstitials in the mechanical behavior of metals // Metallography, Microstructure & Analysis. 2016. Vol. 5. No. 6. Pp. 557–569.

8. **Peral L. B., Zafra A., Fernández-Pariente I., Rodrнguez C., Belzunce J.** Effect of internal hydrogen on the tensile properties of different CrMo(V) steel grades: Influence of vanadium addition on hydrogen trapping and diffusion // International Journal of Hydrogen Energy. 2020. Vol. 45. No. 41. Pp. 22054–22079.

9. **Venezuela J., Hill T., Zhou Q., Li H., Shi Z., Dong F., Knibbe R., Zhang M., Dargusch M. S., Atrens A.** Hydrogen-induced fast fracture in notched 1500 and 1700 MPa class automotive martensitic advanced high-strength steel // Corrosion Science. 2021. Vol. 188. 1 August. P. 109550.

10. **Duportal M., Oudriss A., Savall C., Renaud A., Labrugure-Sarroste C., Feaugas X.** On the implication of mobile hydrogen content on the surface reactivity of an austenitic stainless steel // Electrochimica Acta. 2022. Vol. 403. 20 January. P. 139684.

11. Алексеева Е. Л., Беляев А. К., Зегжда **А. С., Полянский А. М., Полянский В. А., Фролова К. П., Яковлев В. А.** Влияние пограничного слоя на распределение концентраций водорода при испытаниях сталей на стойкость к водородному растрескиванию // Diagnostics, Resource and Mechanics of Materials and Structures. 2018. № 3. С. 43–57.

12. **Polyanskiy V. A., Belyaev A. K., Alekseeva E. L., Polyanskiy A. M., Tretyakov D. A., Yakovlev Yu. A.** Phenomenon of skin effect in metals due to hydrogen absorption // Continuum Mechanics and Thermodynamics. 2019. Vol. 31. No. 6. Pp. 1961–1975.

13. **Martinsson A., Sandström R.** Hydrogen depth profile in phosphorus-doped, oxygen-free copper after cathodic charging // Journal of Materials Science. 2012. Vol. 47. No. 19. Pp. 6768–6776.

14. **Wu R., Ahiström J., Magnusson H., Frisk K., Martinsson E.** Charging, degassing and distribution of hydrogen in cast iron (report SKB R-13-45). Stockholm: Svensk Kärnbränslehantering AB. Swedish Nuclear and Waste Management Co., May 2015. 47 p.

15. **Oriani R. A.** A mechanistic theory of hydrogen embrittlement of steels // Berichte der Bundesgesellschaft für physikalische Chemie. 1972. Vol. 76. No. 8. Pp. 848–857.

16. **Troiano A. R.** The role of hydrogen and other interstitials in the mechanical behavior of metals // Transactions of the American Society of Metals (ASM). 1960. Vol. 52. Pp. 54–80.

17. **Birnbaum H. K., Sofronis P.** Hydrogen-enhanced localized plasticity – a mechanism for hydrogen-related fracture // Materials Science and Engineering A. 1994. Vol. 176. No. 1–2. Pp. 191–202.

18. **Sofronis P.**, **Birnbaum H. K.** Mechanics of the hydrogen dislocation-impurity interactions. I. Increasing shear modulus // Journal of the Mechanics and Physics of Solids. 1995. Vol. 43. No. 1. Pp. 49–90.

19. **Taha A., Sofronis P.** A micromechanics approach to the study of hydrogen transport and embrittlement // Engineering Fracture Mechanics. 2001. Vol. 68. No. 6. Pp. 803–837.

20. Фика закон // Физический энциклопедический словарь. Гл. ред. А. М. Прохоров. М.: Советская энциклопедия, 1984. С. 818.

21. **Шьюмон П.** Диффузия в твердых телах. М.: Металлургия, 1966. 196 с.

22. **Колачев Б. А.** Водородная хрупкость металлов. М.: Металлургия, 1985. 216 с.

23. **Gorsky W.** Theorie der elastischen Nachwirkung in ungeordneten Mischkristallen (elastische Nachwirkung zweiter Art) // Physikalische Zeitschrift der Sowjetunion. 1935. Bd. 8. S. 457–471.

24. **Serebrinsky S., Carter E. A., Ortiz M.** A quantum-mechanically informed continuum model of hydrogen embrittlement // Journal of the Mechanics and Physics of Solids. 2004. Vol. 52. No. 10. Pp. 2403–2430.

25. **McLean D.** Grain boundaries in metals. London: Clarendon Press, 1957. 346 p.

26. **Irwin G. R.** Analysis of stresses and strains near the end of a crack traversing a plate // Journal of Applied Mechanics. 1957. Vol. 24. No. 3. Pp. 361–364.

27. **Irwin G. R.** Fracture // Encyclopedia of Physics. Ed. by S. Flugge. Vol. 6. Elasticity and Plasticity. Berlin: Springer Verlag, 1958. Pp. 551–590.

28. **Wilkins M. L.** Computer simulation of dynamic phenomena Berlin, Heidelberg: Springer Science & Business Media, 1999. 246 p.

29. Справочник по коэффициентам интенсивности напряжений. Под ред. Ю. Мураками. Пер. с англ. В 2 тт. Т. 2. М.: Мир, 1990. 556 с.

30. **Benthem J. P., Koiter W. T.** Asymptotic approximations to crack problems // Methods of analysis and solutions of crack problems. Ed. by G. C. Sih. Book Series "Mechanics of Fracture". Vol. 1. Dordrecht: Springer, 1973. Pp. 131–178.

31. **Hirth J. P.** Effects of hydrogen on the properties of iron and steel // Metallurgical Transactions A. 1980. Vol. 11. No. 6. Pp. 861–890.

32. **Tvergaard V., Hutchinson J. W.** The relation between crack growth resistance and fracture process parameters in elastic-plastic solids // Journal of the Mechanics and Physics of Solids. 1992. Vol. 40. No. 6. Pp. 1377–1397.

33. **Herms E., Olive J. M., Puiggali M.** Hydrogen embrittlement of 316L type stainless steel // Materials Science and Engineering A. 1999. Vol. 272. No. 2. Pp. 279–283.

34. **Momotani Y., Shibata A., Terada D., Tsuji N.** Effect of strain rate on hydrogen embrittlement in low-carbon martensitic steel // International Journal of Hydrogen Energy. 2017. Vol. 42. No. 5. Pp. 3371–3379.

THE AUTHORS

SEDOVA Yuliya S.
Institute for Problems in Mechanical Engineering of the Russian Academy of Sciences
61 Bolshoy Ave., V. Isl.., St. Petersburg, 199178, Russia
sedova.yus@mail.ru
ORCID: 0000-0003-4397-6073

BESSONOV Nikolay M.
Institute for Problems in Mechanical Engineering of the Russian Academy of Sciences
61 Bolshoy Ave., V. Isl.., St. Petersburg, 199178, Russia
nickbessonov1@gmail.com.ru
ORCID: 0000-0001-6462-5980

POLYANSKIY Vladimir A.
Institute for Problems in Mechanical Engineering of the Russian Academy of Sciences
61 Bolshoy Ave., V. Isl.., St. Petersburg, 199178, Russia
vapol@mail.ru
ORCID: 0000-0002-1199-1028

СВЕДЕНИЯ ОБ АВТОРАХ

СЕДОВА Юлия Сергеевна – *стажер-исследователь Института проблем машиноведения Российской академии наук.*
199178, Россия, г. Санкт-Петербург, Большой проспект В. О., 61
sedova.yus@mail.ru
ORCID: 0000-0003-4397-6073

БЕССОНОВ Николай Михайлович – *доктор физико-математических наук, главный научный сотрудник Института проблем машиноведения Российской академии наук.*
199178, Россия, г. Санкт-Петербург, Большой проспект В. О., 61
nickbessonov1@gmail.com.ru
ORCID: 0000-0001-6462-5980

ПОЛЯНСКИЙ Владимир Анатольевич – *доктор технических наук, директор Института проблем машиноведения Российской академии наук.*
199178, Россия, г. Санкт-Петербург, Большой проспект В. О., 61
vapol@mail.ru
ORCID: 0000-0002-1199-1028

Received 31.03.2022. Approved after reviewing 30.06.2022. Accepted 01.07.2022.
Статья поступила в редакцию 31.03.2022. Одобрена после рецензирования 30.06.2022. Принята 01.07.2022.